J Membrane Biol (2014) 247:189–200
DOI 10.1007/s00232-013-9624-x

AFM of the Ultrastructural and Mechanical Properties of Lipid-Raft-Disrupted and/or Cold-Treated Endothelial Cells

Li Wu · Jie Huang · Xiaoxue Yu · Xiaoqing Zhou · Chaoye Gan · Ming Li · Yong Chen

Received: 20 May 2013 / Accepted: 26 December 2013 / Published online: 8 January 2014

Abstract The nonionic detergent extraction at 4 °C and the cholesterol-depletion-induced lipid raft disruption are the two widely used experimental strategies for lipid raft research. However, the effects of raft disruption and/or cold treatment on the ultrastructural and mechanical properties of cells are still unclear. Here, we evaluated the effects of raft disruption and/or cold (4 °C) treatment on these properties of living human umbilical vein endothelial cells (HUVECs). At first, the cholesterol-depletion-induced raft disruption was visualized by confocal microscopy and atomic force microscopy (AFM) in combination with fluorescent quantum dots. Next, the cold-induced cell contraction and the formation of end-branched filopodia were observed by confocal microscopy and AFM. Then, the cell-surface ultrastructures were imaged by AFM, and the data showed that raft disruption and cold treatment induced opposite effects on cell-surface roughness (a significant decrease and a significant increase, respectively). Moreover, the cell-surface mechanical properties (stiffness and adhesion force) of raft-disrupted- and/or cold-treated HUVECs were measured by the force measurement function of AFM. We found that raft disruption and cold treatment induced parallel effects on cell stiffness (increase) or adhesion force (decrease) and that the combination of the two treatments caused dramatically strengthened effects. Finally, raft disruption was found to significantly impair cell migration as previously reported, whereas temporary cold treatment only caused a slight but nonsignificant decrease in cell migration performed at physiological temperature. Although the mechanisms for causing these results might be complicated and more in-depth studies will be needed, our data may provide important information for better understanding the effects of raft disruption or cold treatment on cells and the two strategies for lipid raft research.

Keywords Lipid rafts · Atomic force microscopy (AFM) · Human umbilical vein endothelial cells (HUVECs) · Cholesterol depletion · Cell stiffness · Adhesion force

L. Wu · J. Huang · X. Yu · X. Zhou · C. Gan · M. Li · Y. Chen (✉)
Nanoscale Science and Technology Laboratory, Institute for Advanced Study, Nanchang University, 999 Xuefu Ave., Honggutan District, Nanchang 330031, Jiangxi, China
e-mail: dr_yongchen@hotmail.com

L. Wu · J. Huang · C. Gan · M. Li · Y. Chen
School of Life Sciences and Food Engineering, Nanchang University, Nanchang 330031, Jiangxi, China

Introduction

Lipid raft is a nanoscale (10–200 nm in diameter), floating-raft-like, dynamic cellular structure or microdomain enriched with sterol (cholesterol for animal cells) and sphingolipids (especially gangliosides) (Pike 2006). The specific structure exists mainly in the plasma membrane of most cell types and generally sequesters certain proteins but excludes others or sequesters a protein at a certain status (e.g., resting) but excludes it at another status (e.g., activated) or vice versa. Reasonably, moreover, tiny lipid rafts can be stabilized to form larger nano- or even microclusters. Therefore, this cellular structure has been speculated and then proved to be a platform for molecule sorting, molecule–molecule interaction, and cell signaling (Lingwood and Simons 2010; Pike 2006). After a decade of intensive research, lipid raft has been found to be related to many diseases (Michel and Bakovic 2007; Pike 2006), including viral/bacterial

infection, parasite pathogenesis, cardiovascular diseases (e.g., atherosclerosis), neurological diseases (e.g., Alzheimer's disease), carcinogenesis, and others. In the case of endothelial cell biology, most recently, some studies have explored the important relevance of membrane cholesterol and lipid rafts, with implications for relevant pathways, e.g., vascular endothelial growth factor receptor 2 (VEGFR-2), controlling angiogenesis, development, and diseases (e.g., cardiovascular diseases and cancers) (Fang et al. 2013; Noghero et al. 2012).

Until now, however, a consensus on the lipid raft size is hard to be reached due to a broad range of raft size obtained by different methods or even by a same method. Moreover, there are still some nonbelievers with respect to the existence of lipid rafts due to controversial experimental designs (Munro 2003; Shaw 2006). During lipid raft research, the nonionic detergent extraction at a low temperature (generally 4 °C) and the cholesterol-depletion-induced lipid raft disruption are the two widely used experimental strategies which are also most controversial due to the potentially multiple, multifarious, and multifaceted effects of cholesterol depletion or cold treatment. Presently, it is impossible to make a comprehensive evaluation of the effectiveness of cholesterol depletion or cold treatment in lipid raft research. The aim of this study is not to provide any evidence or implications against the lipid raft concept. This study just used atomic force microscopy (AFM) to investigate the cholesterol-depletion- and/or cold-treatment-induced changes in ultrastructural and mechanical properties of endothelial cells in order to add more information for better understanding the effects of cholesterol depletion and/or cold treatment.

Materials and Methods

Cells and Reagents

Human umbilical vein endothelial cells (HUVECs), purchased from Xiangya Central Experiment Laboratory (Hunan, China), were cultured in DMEM (Gibco) supplemented with 10 % (w/v) fetal calf serum (HyClone, South Logan, UT), 100 U/ml penicillin, and 100 μg/ml streptomycin in 6-well plates or on fresh sterile glass coverslips. For all experiments, cell cultures had been passaged approximately 5 times. Biotinylated CTB (cholera toxin B subunit), MβCD, and streptavidin-conjugated Qdot 655 were purchased from Invitrogen.

Cell-Surface Staining of Ganglioside GM1

HUVECs (2–3 × 10^4/ml) in a petri dish were cultured for 24 h in a CO_2 incubator (37 °C, 5 % CO_2). For the cholesterol depletion experiments, the cells were incubated with 10 mM MβCD in DMEM for an additional 30 min. The cells with or without MβCD treatment were rinsed twice by phosphate-buffered saline (PBS), fixed by 4 % paraformaldehyde for 30 min, and washed again by PBS. Subsequently, the cells were stained by biotinylated CTB (2 μg/ml; 4 °C overnight) and streptavidin-conjugated Qdot 655 (10 nM; 37 °C for 2 h) sequentially. Three washes with PBS were performed after each staining.

Imaging of Ganglioside GM1 on HUVECs Treated With or Without MβCD

For fluorescence imaging, an LSM710 confocal microscope (Carl Zeiss, Oberkochen, Germany) equipped with a Zeiss inverted microscope was used. A Zeiss Plan-Neofluar objective (40 × /0.75) was recruited. For Qdot 655, the excitation wavelength and the emission filter were 405 and 508–690 nm, respectively.

For topographical imaging at the nanometer scale, an Agilent series 5500 AFM (Agilent Technologies, CA) was recruited. The fixed cells (unstained cells without MβCD treatment, stained cells treated without MβCD, and stained cells treated with MβCD) in petri dish were washed twice with distilled water, dried in air, and mounted onto the XY stage of the AFM with an integral video monitor. With $Si3N_4$ tips, the high-resolution images (1 μm × 1 μm) of cell-surface ultrastructures were taken in air in the tapping mode at a scan rate of 0.5 Hz.

Imaging of Cold-Induced Cell Contraction and Filopodium Formation

For dynamical observation of the cold-induced cell contraction of HUVECs by confocal microscopy, the same procedure was used as previously described (Zeng et al. 2013). Briefly, a petri dish with fully spread HUVECs was taken from a CO_2 incubator and mounted on the stage of the confocal microscope equipped with a mini-cell cultivation system (5 % CO_2). After an image of a field of cells at 37 °C was taken, the medium in the petri dish was quickly replaced with prechilled (4 °C) medium. Then, the cold-induced contraction of individual cells in the same field was imaged every 0.5 min for a period of 20 min.

For imaging the cold-induced contracted cells with many cold-induced filopodia at higher spatial resolution, an AutoProbe CP Research AFM (Veeco, Santa Barbara, CA) was utilized. The fully spread HUVECs on glass coverslips were treated with prechilled (4 °C) PBS for 15 min, fixed by 4 % formaldehyde for 20 min, and washed twice by distilled water. The cells on coverslips were air-dried and subjected to AFM imaging in tapping mode. The length, width, and thickness of the silicon nitride AFM cantilevers

(UL20B, Park Scientific Instruments, Sunnyvale, CA) were 115, 30, and 3.5 μm, respectively, with a resonant frequency of 255 kHz and a force constant of 0.03 N/m.

Imaging of Cell-Surface Ultrastructures and Quantification of Cell-Surface Roughness

Four groups of samples were prepared as follows: (a) the cells without treatments; (b) the cells treated by 10 mM MβCD in DMEM at 37 °C for 30 min; (c) the cells treated by prechilled (4 °C) DMEM for 15 min; and (d) the cells were treated by 10 mM MβCD for 30 min, rinsed twice with PBS, and then treated with prechilled (4 °C) DMEM for 15 min. Subsequently, all samples were fixed by 4 % paraformaldehyde for 30 min, dried in air shortly, and then subjected to AFM (Agilent series 5500) imaging in tapping mode. After an individual whole cell was imaged, multiple local areas of 3 μm × 3 μm on the cell were imaged again by AFM, based on which the cell-surface roughness of each local area was extracted by the software equipped with the instrument. The length, width, and thickness of the AFM cantilevers were 225, 38, and 7 μm, respectively, with a resonant frequency of 190 kHz and a force constant of 48 N/m.

Force Measurement

Four groups of samples were prepared as above. However, the cells were unfixed and left alive. Then, the living cells in DMEM were immediately measured by Agilent series 5500 AFM in contact mode. For each cell (≥5 cells in each group), force measurement of an area of 30 μm × 30 μm on the cell surface was performed. For each area, more than 256 force-versus-distance curves were taken, from which the values of cell stiffness and adhesion force were extracted by the instrument software as described previously (Jin et al. 2012). The length and width of the triangular AFM cantilevers were 200 and 28 μm (for each arm), respectively, with a resonant frequency of 77 kHz. The spring constant (∼0.04 N/m) for each cantilever was determined from the measurement of its resonant frequency by a method implemented in the instrument software.

Cell Migration Assay

Cell migration assays were performed using 24-well transwells with 6.5 mm, 8.0 μm pore size inserts (Corning, USA) according to the manufactory's instruction. HUVECs were serum-starved for 12 h. After trypsinization, approximately 5×10^4 cells were added onto the upper face of the transwell insert in 100 μl of DMEM. Then, 600 μl of DMEM at 37 or 4 °C with or without 10 mM MβCD was added to the well and treated for 30 min. After replacement of fresh medium, the cells were allowed to migrate at 37 °C for 24 h after which a cotton swab was used to remove nonmigrant cells at the top of the transwell insert. The migrant cells at the lower face of the insert were fixed in 4 % paraformaldehyde for 20 min and stained with 0.1 % crystal violet for 30 min at room temperature. After gentle washes with distilled water to remove excess dyes on the surface of the filter, migrated cells were quantified in five random fields.

Data Processing and Statistical Analysis

PicoView 1.12 equipped with Agilent series 5500 AFM was used to analyze AFM images and force-versus-distance curves. GraphPad Prism version 5.0 (GraphPad Software, La Jolla, CA) was used to make all graphs. The distribution histograms were made by EasyFit 5.5 (MathWave Technologies, Dnepropetrovsk, Ukraine). For all data, at least three independent experiments were conducted. All values are expressed as mean ± SD. Statistic analyses were conducted using Student's *t* test to determine the significance between different groups. It was regarded as significant difference when $p < 0.05$.

Results

Cholesterol-Depletion-Induced Disruption of Lipid Rafts in the Plasma Membrane

Cholesterol depletion is the most widely used method for inducing the disruption of lipid rafts. To confirm that cholesterol depletion induced lipid raft disruption, we utilized biotinylated cholera toxin unit B (CTB) to label ganglioside GM1, a putative lipid marker of lipid rafts in the plasma membrane, following with the staining of streptavidin-conjugated fluorescent quantum dots (Qdot 655), which can function as both a fluorescent and topographical probe in confocal and AFM, respectively (Wang et al. 2009a, b). Confocal fluorescence images show that compared with untreated cells, the cell-surface GM1 staining on cholesterol-depleted HUVECs by MβCD became worse (Fig. 1a), implying that the lipid rafts in the plasma membrane of the treated HUVECs have been disrupted to some degree.

To further confirm the result on the nanometer scale, we used AFM to image the cell surfaces of treated or untreated cells with or without cell-surface staining. The biocompatible fluorescent quantum dots (Qdot 655) have a spherical or subsphaeroidal shape and a size of approximately 20 nm in diameter (Chen et al. 2008; Pierobon and Cappello 2012), which are probably detectable by high-

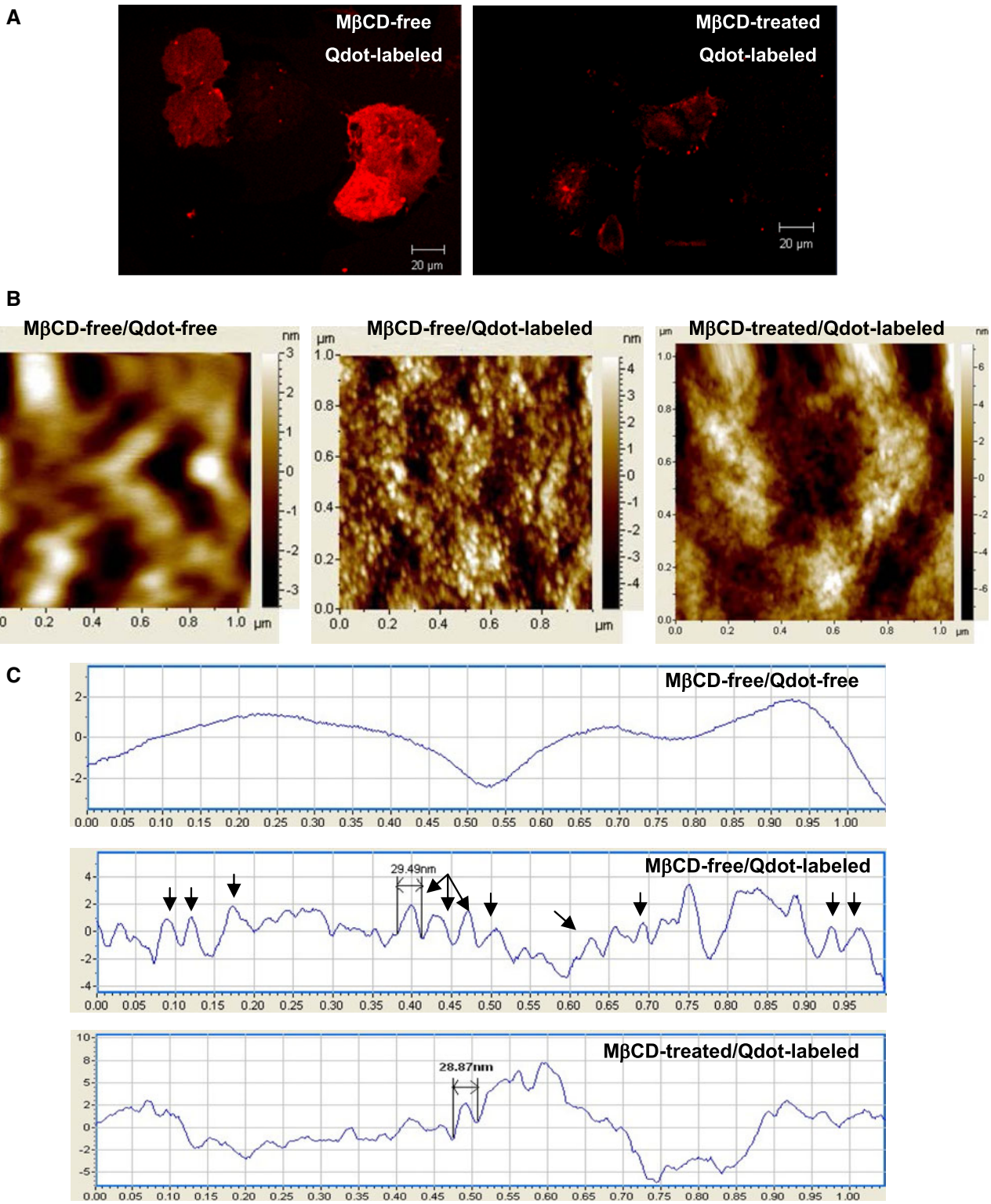

resolution AFM. Obviously, the wavy surface of the untreated cells without staining is very smooth (the left panel of Fig. 1b and the upper panel of Fig. 1c), whereas after stained with quantum dots, many spherical or subsphaeroidal particles with a similar size to that of quantum dots appeared on the wavy surface of untreated cells (the middle panels of Fig. 1b, c). Upon cholesterol depletion by MβCD, the number of nanoscale particles on the wavy surface decreased clearly (the right panel of Fig. 1b and the bottom panel of Fig. 1c), implying the decrease in the

◀**Fig. 1** Disruption of lipid rafts in the plasma membrane of HUVECs induced by cholesterol depletion. **a** Confocal fluorescence images of GM1 (a lipid raft marker) on MβCD-free (*left*) and MβCD-treated (*right*) cells stained with biotinylated CTB and fluorescent quantum dot (Qdot 655)-conjugated streptavidin. *Scale bar* 20 μm. **b** AFM topographical images of cell-surface ultrastructures of HUVECs treated with or without MβCD and stained with or without CTB/Qdot 655. *Scan area* approximately 1 μm × 1 μm. The *scale bar* at the *right side* of each AFM image shows the vertical range of the image, with darkest point of the bar corresponding to the lowest measured point and the upper limit of the bar to the highest measured point. **c** Height profiles of cross sections horizontally across the topographical images. Compared with the label-free control (*left* in **b** and *upper* in **c**) and the MβCD-treated cell (*right* in **b** and *bottom* in **c**), many small particles with a size of approximately 20–30 nm (as indicated by the *arrows* in the *middle panel* of **c**) display on the MβCD-free, Qdot-labeled cell (*middle* in **b**, **c**)

number of cell-surface GM1 and, in other words, the disruption of lipid rafts.

Cold-Treatment-Induced Cell Contraction and Transformation of Lamellipodia into End-Branched Filopodia

Prior to the investigation on the cold-induced changes in ultrastructural and mechanical properties of cells, the effects of cold treatment on individual whole cells were studied. Cold-induced cell contraction is a well-known phenomenon which has also been documented in our previous studies (Huang et al. 2012; Zeng et al. 2013) and was confirmed again by confocal microscopy in this study (Fig. 2a). Interestingly, during the course of cold-induced cell contraction, the lamellipodia of spread cells (the left panel of Fig. 2a) is transformed into many filopodia (the right panel of Fig. 2a).

To visualize and quantify the filopodia, for the first time, AFM was recruited to image and measure the ends of cold-induced filopodia. We found that there is a root-like structure at the end of each filopodium (Fig. 2b). It is perhaps a structure of attachment, probably composed of stress fibers and focal adhesions by which a cell is attached onto a substrate. The branches have a height of approximately 20–30 nm and a diameter of 200–300 nm for the last-level branches (the upper panel of Fig. 2c) or a height of approximately 40 nm and a diameter of 500–1,000 nm for the following-level branches (the lower panel of Fig. 2c).

Lipid Raft Disruption and Cold Treatment Resulted in Opposite Effects on Cell-Surface Roughness

As previously observed (Liao et al. 2014; Shao et al. 2013), there exist three regions with different degrees of roughness on the cell surface of cultured HUVECs (Fig. 3a). Therefore, after a single whole cell was imaged by AFM, an AFM topographical image of 3 μm × 3 μm was taken in each of the three regions (R1, R2, and R3, respectively) on the cell (Fig. 3b), following with the extraction of the data on average roughness for statistical analysis (Fig. 3c). We found that lipid raft disruption and cold treatment resulted in opposite effects on cell-surface roughness. Obviously in Fig. 3c, lipid raft disruption induced a significant decrease, whereas cold treatment caused a significant increase in the cell-surface average roughness of each of the three regions (especially region 2).

Lipid Raft Disruption and Cold Treatment Resulted in Parallel Effects on Mechanical Properties

Next, we used the force measurement functions of AFM to investigate the effects of lipid raft disruption and/or cold treatment on cellular mechanical properties including stiffness and adhesion force (Figs. 4, 5). The force measurements were performed in an area of 30 μm × 30 μm, and approximately 256 points per area were detected for force-versus-distance curves which were used to make the representative images (Figs. 4a, 5a, respectively), distribution graphs (Figs. 4b, 5b, respectively), and histograms (Figs. 4c, 5c, respectively) of biomechanical properties (stiffness and adhesion force, respectively). The stiffness data indicate that both cholesterol-depletion-induced raft disruption and cold treatment caused significant increases in stiffness (Fig. 4).

The adhesion property of endothelial cells is vital for their attachment on a substrate or for the attachment of blood cells or cancer cells on endothelial cells or endothelium. Therefore, we sought to investigate the effects of raft disruption and/or cold treatment on the adhesion property of HUVECs by measuring the adhesive forces between AFM tips and cell surfaces. AFM data indicate that both lipid raft disruption and cold treatment induced significant decreases in adhesive force (Fig. 5).

Combination of Cold Treatment with Raft Disruption Exerted Dramatic Effects on Mechanical Properties

During experiments of lipid raft extraction at 4 °C, the cholesterol-depletion-induced lipid raft disruption is often performed as a negative control. Therefore, we evaluated the combined effects of raft disruption plus cold treatment on the ultrastructural and mechanical properties of HUVECs. The data indicate that the combined effects were in concert with the separate effects and that lipid raft disruption slightly weakened the effect of cold treatment on cell-surface average roughness (Fig. 3c) whereas dramatically strengthened the effects of cold treatment on cell stiffness and adhesion properties (Figs. 4, 5).

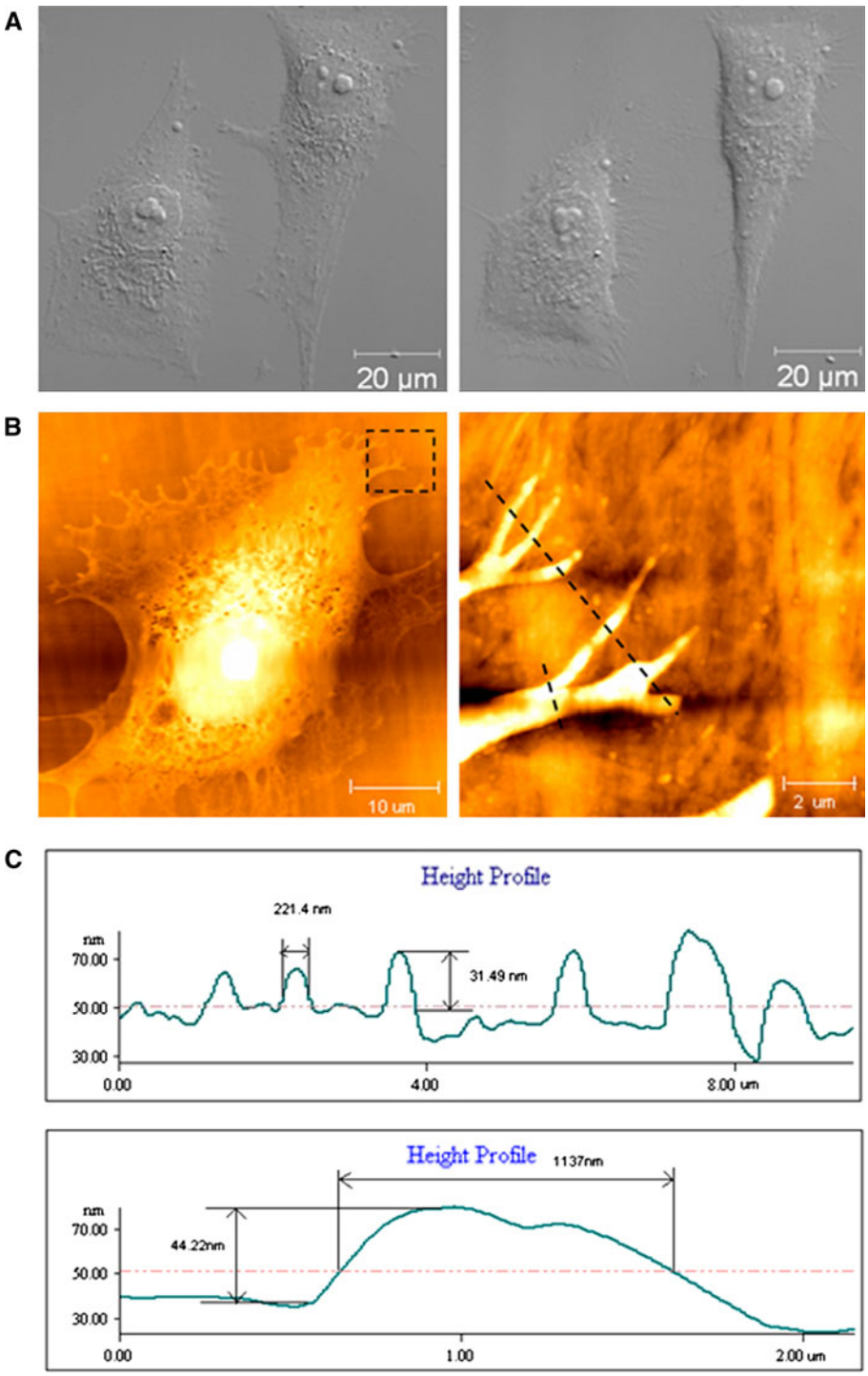

Fig. 2 Cell contraction of HUVECs and formation of filopodia induced by cold treatment. **a** The representative phase-contrast images of two cells before (*left*) and after cold treatment for 20 min. **b** AFM topographical images of a cell treated by cold for 20 min (*left*) and its local region (*right*) enlarged from the *dashed box* in the *left panel*. Many end-branched filopodia are evident clearly. *Scale bars* 10 μm (*left*) and 2 μm (*right*). **c** The *upper* and *lower* height profiles are extracted from the cross sections at the long- and short-dashed lines in the *right panel* of Fig. 2b, respectively, showing the diameters and heights of a filopodium and some branches

Lipid Raft Disruption Resulted in Decreased Migration of HUVECs

Finally, we tested the effects of lipid raft disruption and/or cold treatment on the migration of HUVECs using 24-well transwells. The data indicate that lipid raft disruption significantly impaired the migration of HUVECs, whereas cold treatment weakened cell migration slightly but not significantly (Fig. 6). Cold treatment of the cells was performed only for 30 min, and then, cell migration assay was conducted at 37 °C for a much longer period. The physiological temperature might reverse the potentially inhibitory effect of cold treatment on cell migration which should be responsible for the statistically nonsignificant data.

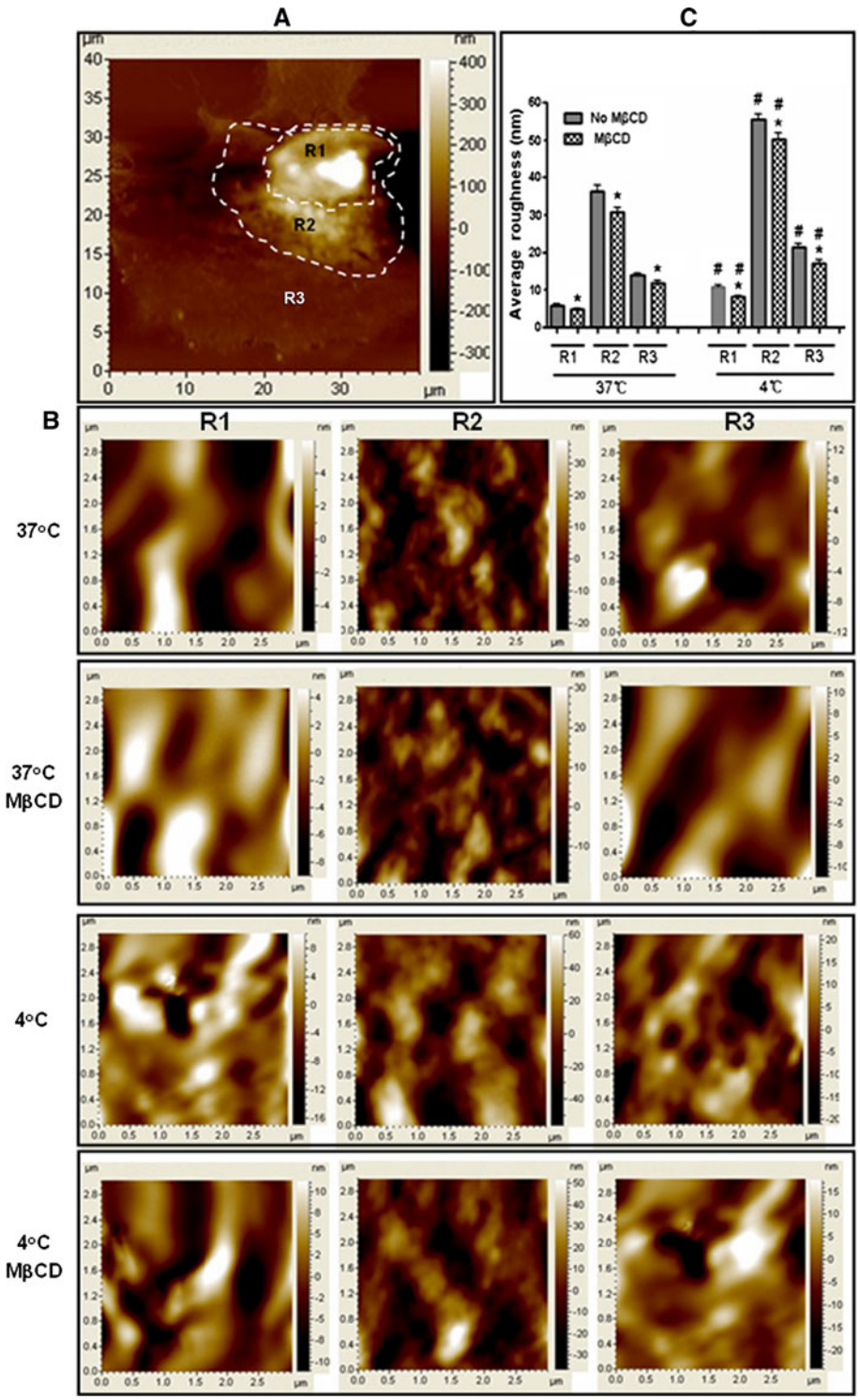

Fig. 3 Effects of cholesterol depletion and/or cold treatment on cell-surface roughness of HUVECs. **a** Three regions with different degrees of roughness were indicated by "R1," "R2," and "R3," respectively, on the representative AFM topographical image of a cell. **b** Representative AFM topographical images of local areas (3 μm × 3 μm) in the three regions (R1–R3) under different conditions showing the changes in cell-surface roughness. From the *upper panel* to the *bottom panel* no treatment; cholesterol depletion; cold treatment; cholesterol depletion and then cold treatment. **c** The histogram graph showing the changes in average roughness. "*," $p < 0.05$ when comparing cholesterol depletion groups with the corresponding groups of no cholesterol depletion; "#," $p < 0.05$ when comparing cold treatment groups with the corresponding groups of no cold treatment

Discussion

The nonionic detergent extraction at 4 °C and the cholesterol-depletion-induced lipid raft disruption are the two main approaches for lipid raft research, whereas it has been a long-standing question what effects cold treatment or raft disruption may have on cellular structures or functions. The effects of cholesterol depletion have been widely studied, and many structures and cellular processes have been found to be influenced by cholesterol depletion, including membrane depolarization, membrane permeability, protein diffusion or immobilization, endocytosis, Ca2+-dependent responses, induction of autophagy, signaling transduction, among

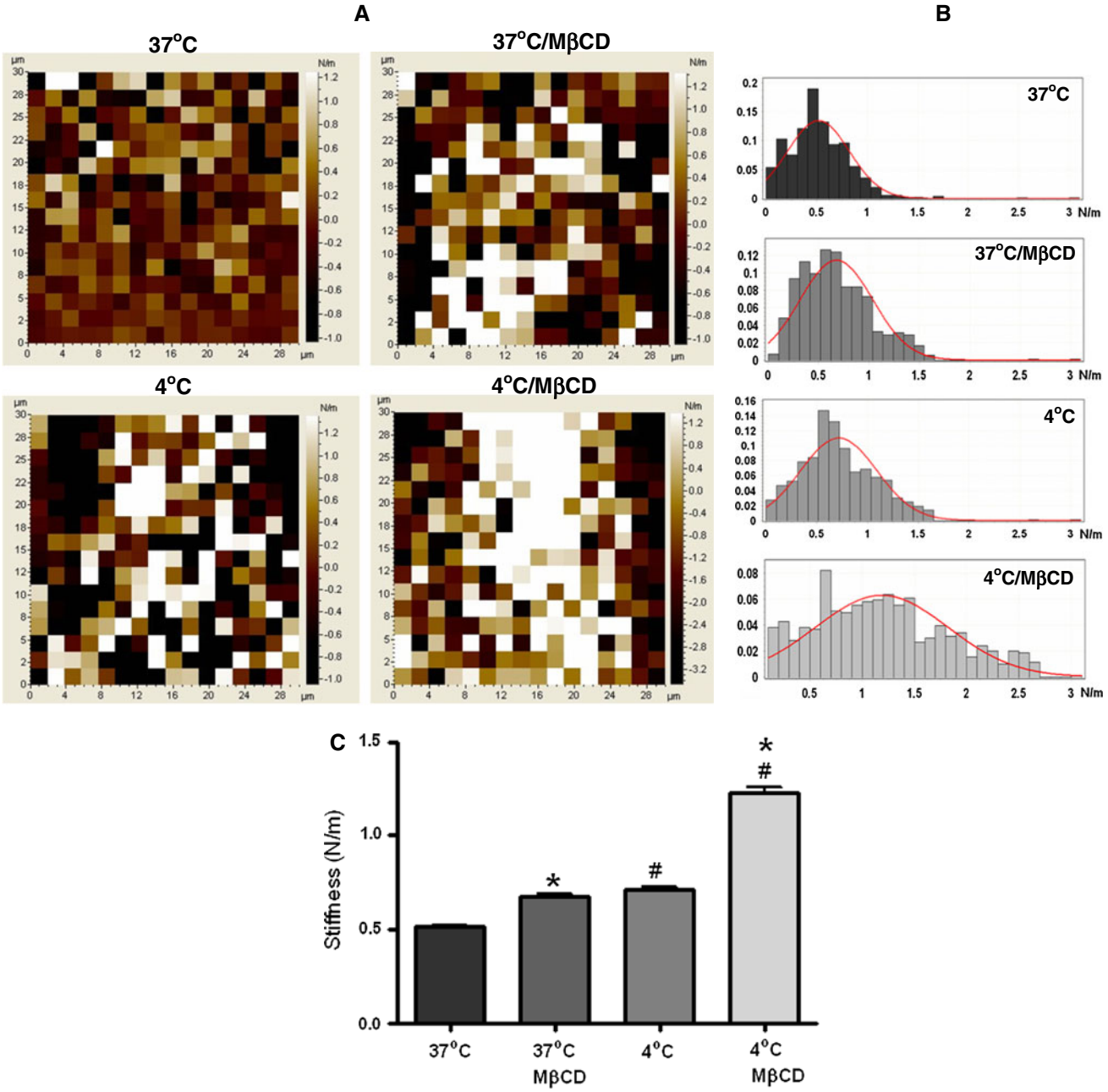

Fig. 4 Effects of cholesterol depletion and/or cold treatment on cell-surface stiffness of HUVECs. **a** Cell stiffness mapping on a 30 μm × 30 μm surface area of cells showing the cholesterol-depletion- and/or cold-induced changes in cell stiffness. The *scale bar* at the *right side* of each AFM image shows the vertical range of the image, with darkest point of the bar corresponding to the smallest stiffness and the upper limit of the bar to the largest stiffness. **b** The corresponding stiffness distributions. **c** The histogram graph. "*," $p < 0.05$ when comparing cholesterol depletion groups with the corresponding groups of no cholesterol depletion; "#," $p < 0.05$ when comparing cold treatment groups with the corresponding groups of no cold treatment

others (Kenworthy 2008; Munro 2003). However, the effects of cholesterol depletion on ultrastructural (average cell-surface roughness) and/or mechanical (cell stiffness and adhesion force) properties of cells are less investigated.

On the other hand, it is also well known that lipid phase behavior is highly temperature dependent and that the reduction in temperature could potentially induce alternations in many respects (Rubinsky 2003). However, the effects of cold treatment on those properties are also relatively less evaluated. Interestingly, for the first time, using AFM, we found that besides cell contraction, cold treatment also induced the formation of end-branched filopodia (Fig. 2), at least temporarily. We speculate that

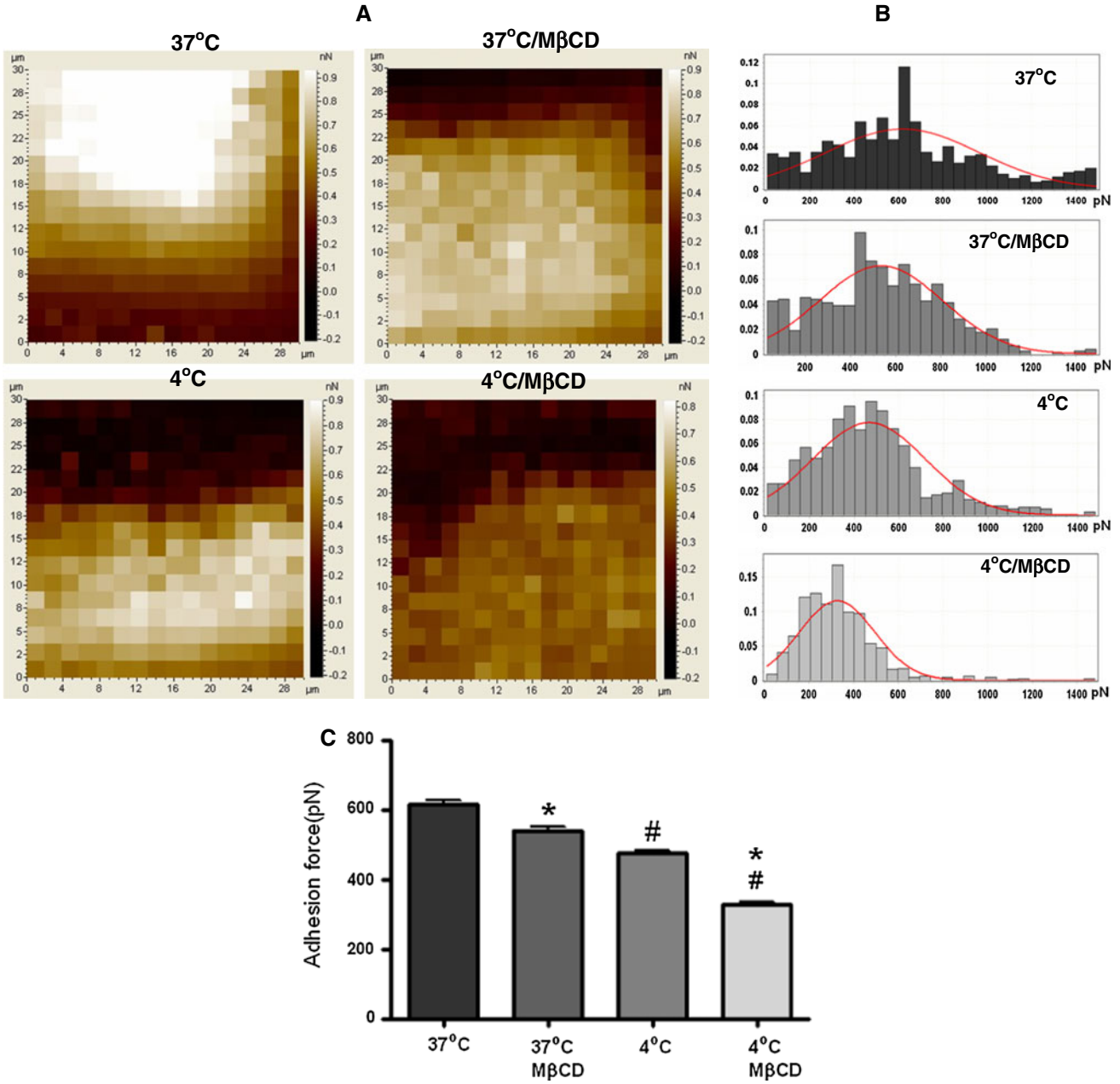

Fig. 5 Effects of cholesterol depletion and/or cold treatment on cell-surface adhesion force of HUVECs. **a** Adhesion force mapping on a 30 μm × 30 μm surface area of cells showing the cholesterol-depletion- and/or cold-induced changes in cell-surface adhesion force. The *scale bar* at the *right side* of each AFM image shows the vertical range of the image, with darkest point of the bar corresponding to the weakest adhesion force and the upper limit of the bar to the strongest force. **b** The corresponding adhesion force distributions. **c** The histogram graph. "*," $p < 0.05$ when comparing cholesterol depletion groups with the corresponding groups of no cholesterol depletion; "#," $p < 0.05$ when comparing cold treatment groups with the corresponding groups of no cold treatment

cold-induced rapid contraction of a lamellipodium drove the adduction of 2–3 or more adjacent stress fibers to form individual bundles with a larger size as measured, whereas the cold-induced detachment of focal adhesions at the ends of stress fibers from the substrate might lag behind the cold-induced adduction of adjacent stress fibers, which caused the formation of the root-like structure at the end of each filopodium. More in-depth research will be needed to verify the speculation.

Some conceivable possibilities might cause the change in cell-surface roughness (or the degree of micrometer- or nanometer-scale surface undulation of the plasma membrane): (a) alternation in amount of proteins with relatively large sizes at the outer leaflet of the plasma membrane;

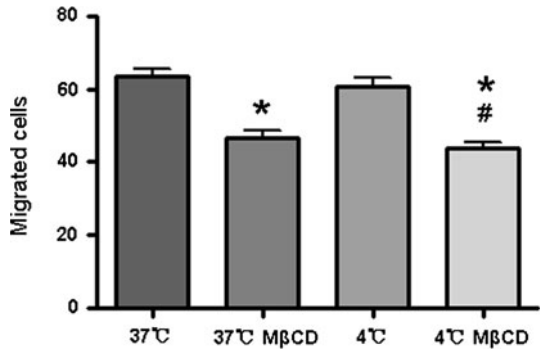

Fig. 6 Effects of cholesterol depletion and/or cold treatment on cell migration of HUVECs investigated using transwells. The histogram graph shows the average number of migrated cells per field in each group. "*," $p < 0.05$ versus the 37 °C group; "#," $p < 0.05$ versus the 4 °C group

(b) aggregation (e.g., recognition- or cross-linking-induced aggregation) of membrane-bound molecules into larger clusters or dispersion of large clusters; (c) appearance/increase or disappearance/decrease in some cell-surface ultrastructures, such as microvillus, membrane folds or ruffles, membrane curvatures, membrane vesicles, and exocytotic fusion pores; (d) rearrangement of the cytoskeleton (e.g., cell spreading, cell contraction, and others; the formation of the above-mentioned cell-surface ultrastructures is also generally driven by the rearrangement of the cytoskeleton but to a relatively low degree). It seems that the latter two will influence the cell-surface roughness more dramatically than the former two.

Since the effects of cholesterol depletion on cellular processes are very complicated, it is hard to exactly explain how cholesterol depletion caused the decrease in cell-surface roughness (Fig. 3). The reasons might be multifarious and combined. As a signaling platform, lipid rafts are generally stabilized by forming nano- or microclusters. Cholesterol depletion might disrupt the clusters, therefore contributing to the decrease in membrane roughness. It has been reported that lipid raft plays important role in membrane curvature and vesicle budding (Frick et al. 2007; Huttner and Zimmerberg 2001). It was possible that raft disruption lowered membrane roughness by influencing the formation of membrane curvature and/or vesiculation. Moreover, lipid rafts have been found to be connected with the cytoskeleton (Lillemeier et al. 2006), and raft disruption by cholesterol depletion could affect the membrane–cytoskeleton adhesion (Sun et al. 2007) and therefore also responsible for the change in cell-surface roughness.

Many factors were also potentially involved in the cold-induced increase in cell-surface roughness (Fig. 3) since cold treatment has been reported to dramatically induce the increase in free cytosolic calcium level (Winokur and Hartwig 1995), the coalescence of membrane microdomains (Chen et al. 2009; Magee et al. 2005), and increased membrane vesiculation (Bode and Knupp 1994). However, the major determinant should be the cold-induced, cytoskeleton-driven, tremendous contraction of the well-spread cells (Fig. 2), which might cause increased membrane reservoir by membrane folding or formation of membrane projections in order to balance the membrane area (Mounier et al. 1999; Raucher and Sheetz 1999; Staykova et al. 2011).

Concerning the enhancement effects of cholesterol depletion on cell stiffness, our data on HUVECs coincide with the previously reported data on bovine aortic endothelial cells (BAECs) detected by micropipette aspiration (Byfield et al. 2004). The underlying mechanism has been elucidated to be the enhancement of membrane–cytoskeleton adhesion but not plasma membrane stiffening (Byfield et al. 2004; Norman et al. 2010; Sun et al. 2007).

As for the effects of cold treatment on cell stiffness, we predicted a decrease in stiffness of cold-treated cells since the cold-induced cell contraction seems like a process contrary to cell spreading during which cell stiffness has been reported to increase gradually (Bhadriraju and Hansen 2002; Roca-Cusachs et al. 2008; Wang and Ingber 1994). Surprisingly, but interestingly, cold treatment caused a significant increase in cell stiffness of HUVECs (Fig. 4). The opposite influences perhaps imply a different underlying mechanism of cold-induced cell contraction from that of natural cell de-spreading. Indeed, it has been reported that disruption of F-actin assembly lowers both spreading and stiffness, whereas disruption of myosin inhibits cell spreading but increases cell stiffness (Bhadriraju and Hansen 2002; Mammoto et al. 2004; Wakatsuki et al. 2003), implying that the cold-induced increase in cell stiffness is potentially correlated with myosin. More in-depth research will be needed to certify this view.

Since electrostatic interactions between AFM tips and cell surfaces might be majorly responsible for the AFM measurements of cell-surface adhesive force, the net charges of the outer surface of the plasma membrane might be the major determinant for cellular adhesion property. The lipid bilayer's outer leaflet of the plasma membrane consists mainly of phosphatidylcholine (PC), sphingomyelin (SM), cholesterol, and glycolipids, among which the former three do not have net electrostatic charge (Langner and Kubica 1999). Therefore, the electrostatics of the cell surface are mainly determined by the charged carbohydrate residues of glycolipids (e.g., glycosphingolipids) and glycoproteins (e.g., adhesion molecules and receptors) (Langner and Kubica 1999).

It has been known that lipid rafts are enriched with gangliosides (e.g., the putative lipid raft marker ganglioside GM1) (Pike 2006) and that many adhesion molecules, receptors, and lectins are generally associated with lipid rafts (Fullekrug and Simons 2004; Kiely et al. 2003; Lajoie

et al. 2009). The cholesterol-depletion-induced disruption of lipid rafts might lower the electrostatic charges by the impairing of gangliosides (e.g., GM1 as shown in Fig. 1) and adhesion molecules or receptors, therefore causing the decrease in adhesion force (Fig. 5). At present, it is hard to explain the cold-induced decrease in cell-surface adhesion force since cold can induce reduced metabolism, denaturation of proteins, increased intracellular calcium (Rubinsky 2003), as well as coalescence of lipid rafts (Chen et al. 2009; Magee et al. 2005). However, the cold-induced rapid detachment and contraction of cells from the substrate partially reflect the decrease in cell-surface adhesion force. Moreover, many studies have observed that the capacity of cell adhesion is dramatically reduced at low temperatures as compared with the physiological temperature (Juliano and Gagalang 1977; Rico et al. 2010; Sagvolden et al. 1999).

After evaluating the effects on the ultrastructural and mechanical properties of cells, we also investigated the effects of lipid raft disruption and/or cold treatment on cell migration. We found that lipid raft disruption significantly impaired the migration of HUVECs, whereas temporary (for 30 min) cold treatment just slightly but nonsignificantly decreased cell migration. Our data on lipid-raft-disruption-induced inhibition of cell migration coincides with previous studies on cancer cells (Manes et al. 1999; Murai et al. 2011), T cells (Gomez-Mouton et al. 2001), HUVECs (Noghero et al. 2012), and others (Ando et al. 2010). The underlying mechanisms may be related to cell signaling mediated by multiple receptors including VEGFR-2 (Fang et al. 2013; Noghero et al. 2012). It seems that lipid raft disruption can cause prolonged inhibitory effects on cell migration due to the damage of the platform (lipid rafts) for molecule–molecule interactions and cell signaling, whereas temporary cold treatment has no significant effects due to the restoration of cold-induced temporary redistribution/coalescence of lipid rafts or other structures at physiological temperature.

Acknowledgments This study was supported by the National Natural Science Foundation of China (31260205 & 30900340), the Scientific Research Fund of Jiangxi Provincial Education Department (GJJ10305), and the Scientific Research Foundation for Returned Overseas Chinese Scholar of State Education Ministry.

References

Ando K, Obara Y, Sugama J, Kotani A, Koike N, Ohkubo S, Nakahata N (2010) P2Y2 receptor-Gq/11 signaling at lipid rafts is required for UTP-induced cell migration in NG 108-15 cells. J Pharmacol Exp Ther 334:809–819

Bhadriraju K, Hansen LK (2002) Extracellular matrix- and cytoskeleton-dependent changes in cell shape and stiffness. Exp Cell Res 278:92–100

Bode AP, Knupp CL (1994) Effect of cold storage on platelet glycoprotein Ib and vesiculation. Transfusion 34:690–696

Byfield FJ, Aranda-Espinoza H, Romanenko VG, Rothblat GH, Levitan I (2004) Cholesterol depletion increases membrane stiffness of aortic endothelial cells. Biophys J 87:3336–3343

Chen Y, Shao L, Ali Z, Cai J, Chen ZW (2008) NSOM/QD-based nanoscale immunofluorescence imaging of antigen-specific T-cell receptor responses during an in vivo clonal Vgamma2V-delta2 T-cell expansion. Blood 111:4220–4232

Chen Y, Qin J, Cai J, Chen ZW (2009) Cold induces micro- and nanoscale reorganization of lipid raft markers at mounds of T-cell membrane fluctuations. PLoS One 4:e5386

Fang L, Choi SH, Baek JS, Liu C, Almazan F, Ulrich F, Wiesner P, Taleb A, Deer E, Pattison J et al (2013) Control of angiogenesis by AIBP-mediated cholesterol efflux. Nature 498:118–122

Frick M, Bright NA, Riento K, Bray A, Merrified C, Nichols BJ (2007) Coassembly of flotillins induces formation of membrane microdomains, membrane curvature, and vesicle budding. Curr Biol 17:1151–1156

Fullekrug J, Simons K (2004) Lipid rafts and apical membrane traffic. Ann N Y Acad Sci 1014:164–169

Gomez-Mouton C, Abad JL, Mira E, Lacalle RA, Gallardo E, Jimenez-Baranda S, Illa I, Bernad A, Manes S, Martinez AC (2001) Segregation of leading-edge and uropod components into specific lipid rafts during T cell polarization. Proc Natl Acad Sci USA 98:9642–9647

Huang J, Shao W, Wu L, Yang W, Chen Y (2012) Effects of exogenous ganglioside GM1 on different stages of cell spreading studied by directly quantifying spreading rate. Cell Commun Adhes 19:85–95

Huttner WB, Zimmerberg J (2001) Implications of lipid microdomains for membrane curvature, budding and fission. Curr Opin Cell Biol 13:478–484

Jin H, Pi J, Huang X, Huang F, Shao W, Li S, Chen Y, Cai J (2012) BMP2 promotes migration and invasion of breast cancer cells via cytoskeletal reorganization and adhesion decrease: an AFM investigation. Appl Microbiol Biotechnol 93:1715–1723

Juliano RL, Gagalang E (1977) The adhesion of Chinese hamster cells. I. Effects of temperature, metabolic inhibitors and proteolytic dissection of cell surface macromolecules. J Cell Physiol 92:209–220

Kenworthy AK (2008) Have we become overly reliant on lipid rafts? Talking point on the involvement of lipid rafts in T-cell activation. EMBO Rep 9:531–535

Kiely JM, Hu Y, Garcia-Cardena G, Gimbrone MA Jr (2003) Lipid raft localization of cell surface E-selectin is required for ligation-induced activation of phospholipase C gamma. J Immunol 171:3216–3224

Lajoie P, Goetz JG, Dennis JW, Nabi IR (2009) Lattices, rafts, and scaffolds: domain regulation of receptor signaling at the plasma membrane. J Cell Biol 185:381–385

Langner M, Kubica K (1999) The electrostatics of lipid surfaces. Chem Phys Lipids 101:3–35

Liao H, He H, Chen Y, Zeng F, Huang J, Wu L, Chen Y (2014) Effects of long-term serial cell passaging on cell spreading, migration, and cell-surface ultrastructures of cultured vascular endothelial cells. Cytotechnology. doi:10.1007/s10616-013-9560-8

Lillemeier BF, Pfeiffer JR, Surviladze Z, Wilson BS, Davis MM (2006) Plasma membrane-associated proteins are clustered into islands attached to the cytoskeleton. Proc Natl Acad Sci USA 103:18992–18997

Lingwood D, Simons K (2010) Lipid rafts as a membrane-organizing principle. Science 327:46–50

Magee AI, Adler J, Parmryd I (2005) Cold-induced coalescence of T-cell plasma membrane microdomains activates signalling pathways. J Cell Sci 118:3141–3151

Mammoto A, Huang S, Moore K, Oh P, Ingber DE (2004) Role of RhoA, mDia, and ROCK in cell shape-dependent control of the Skp2-p27kip1 pathway and the G1/S transition. J Biol Chem 279:26323–26330

Manes S, Mira E, Gomez-Mouton C, Lacalle RA, Keller P, Labrador JP, Martinez AC (1999) Membrane raft microdomains mediate front-rear polarity in migrating cells. EMBO J 18:6211–6220

Michel V, Bakovic M (2007) Lipid rafts in health and disease. Biol Cell 99:129–140

Mounier J, Laurent V, Hall A, Fort P, Carlier MF, Sansonetti PJ, Egile C (1999) Rho family GTPases control entry of *Shigella flexneri* into epithelial cells but not intracellular motility. J Cell Sci 112(Pt 13):2069–2080

Munro S (2003) Lipid rafts: elusive or illusive? Cell 115:377–388

Murai T, Maruyama Y, Mio K, Nishiyama H, Suga M, Sato C (2011) Low cholesterol triggers membrane microdomain-dependent CD44 shedding and suppresses tumor cell migration. J Biol Chem 286:1999–2007

Noghero A, Perino A, Seano G, Saglio E, Lo Sasso G, Veglio F, Primo L, Hirsch E, Bussolino F, Morello F (2012) Liver X receptor activation reduces angiogenesis by impairing lipid raft localization and signaling of vascular endothelial growth factor receptor-2. Arterioscler Thromb Vasc Biol 32:2280–2288

Norman LL, Oetama RJ, Dembo M, Byfield F, Hammer DA, Levitan I, Aranda-Espinoza H (2010) Modification of cellular cholesterol content affects traction force, adhesion and cell spreading. Cell Mol Bioeng 3:151–162

Pierobon P, Cappello G (2012) Quantum dots to tail single biomolecules inside living cells. Adv Drug Deliv Rev 64:167–178

Pike LJ (2006) Rafts defined: a report on the Keystone Symposium on Lipid Rafts and Cell Function. J Lipid Res 47:1597–1598

Raucher D, Sheetz MP (1999) Characteristics of a membrane reservoir buffering membrane tension. Biophys J 77:1992–2002

Rico F, Chu C, Abdulreda MH, Qin Y, Moy VT (2010) Temperature modulation of integrin-mediated cell adhesion. Biophys J 99:1387–1396

Roca-Cusachs P, Alcaraz J, Sunyer R, Samitier J, Farre R, Navajas D (2008) Micropatterning of single endothelial cell shape reveals a tight coupling between nuclear volume in G1 and proliferation. Biophys J 94:4984–4995

Rubinsky B (2003) Principles of low temperature cell preservation. Heart Fail Rev 8:277–284

Sagvolden G, Giaever I, Pettersen EO, Feder J (1999) Cell adhesion force microscopy. Proc Natl Acad Sci USA 96:471–476

Shao W, Jin H, Huang J, Qiu B, Xia R, Deng Z, Cai J, Chen Y (2013) AFM investigation on Ox-LDL-induced changes in cell spreading and cell-surface adhesion property of endothelial cells. Scanning 35:119–126

Shaw AS (2006) Lipid rafts: now you see them, now you don't. Nat Immunol 7:1139–1142

Staykova M, Holmes DP, Read C, Stone HA (2011) Mechanics of surface area regulation in cells examined with confined lipid membranes. Proc Natl Acad Sci USA 108:9084–9088

Sun M, Northup N, Marga F, Huber T, Byfield FJ, Levitan I, Forgacs G (2007) The effect of cellular cholesterol on membrane–cytoskeleton adhesion. J Cell Sci 120:2223–2231

Wakatsuki T, Wysolmerski RB, Elson EL (2003) Mechanics of cell spreading: role of myosin II. J Cell Sci 116:1617–1625

Wang N, Ingber DE (1994) Control of cytoskeletal mechanics by extracellular matrix, cell shape, and mechanical tension. Biophys J 66:2181–2189

Wang X, He D, Cai J, Chen T, Zou F, Li Y, Wu Y, Chen ZW, Chen Y (2009a) WGA-QD probe-based AFM detects WGA-binding sites on cell surface and WGA-induced rigidity alternation. Biochem Biophys Res Commun 379:335–340

Wang Y, Chen Y, Cai J, Zhong L (2009b) QD as a bifunctional cell-surface marker for both fluorescence and atomic force microscopy. Ultramicroscopy 109:268–274

Winokur R, Hartwig JH (1995) Mechanism of shape change in chilled human platelets. Blood 85:1796–1804

Zeng F, Yang W, Huang J, Chen Y (2013) Determination of the lowest concentrations of aldehyde fixatives for completely fixing various cellular structures by real-time imaging and quantification. Histochem Cell Biol 139:735–749